# Effect of heat treatment on microstructure and dimensional stability of ZL114A aluminum alloy

JIANG Long-tao(姜龙涛), WU Gao-hui(武高辉), YANG Wen-shu(杨文澍),
ZHAO Yong-gang(赵永刚), LIU Shan-shan(刘珊珊)

School of Materials Science and Engineering, Harbin Institute of Technology, Harbin 150001, China

**Abstract:** The effects of heat treatment process on microstructure, micro-yield strength and dynamic dimensional stability of ZL114A aluminum alloy were investigated by optical microscopy (OM), transmission electron microscopy (TEM), tensile testing and thermal cycling on-line measuring method. Fine dispersed eutectic Si phases are observed, and long strip eutectic Si and massive primary Si phases decrease in ZL114A alloy after high-temperature and long-time solution treatment, which result in the increase of micro-plastic deformation resistance. With the increasing of aging temperature, aging precipitation behaviour of ZL114A alloy transforms from precipitation of GP zone and $\beta'$ phases simultaneously at lower temperature to precipitation of stable $Mg_2Si$ phases at higher temperature. Because coherent strengthening is the main strengthen mechanism for micro-plastic deformation, precipitation of stable $Mg_2Si$ phases is unfavorable to the improvement of micro-plastic deformation resistance. Micro-yield strength cannot characterize dimensional stability comprehensively, and dynamic dimensional stability under alternative temperature should also be tested cooperatively for better evaluation of dimensional stability.

**Key words:** ZL114A alloy; microstructure; heat treatment; dimensional stability

## 1 Introduction

ZL114A alloy is high strength Al-Si-Mg casting aluminum alloy, which is produced by adding a certain amount of Mg into Zl101A alloy. $\alpha$ solid solution, ($\alpha$+Si) eutectic phase, $Mg_2Si$ and Fe-based compounds, etc are the main phases of ZL114A alloy[1−3].

Vast researches reveal that improving synthetical mechanical properties of ZL114A alloy by adjusting heat treatment process is one of the high spots. Optimum heat treatment process is determined by adjusting the solution temperature[4−5], solution time[4−6], quenchant[4, 7−8], aging temperature[8−9] and aging time to obtain superior mechanical properties.

ZL114A alloy has been wildly used in inertial instrument because of its superior mechanical properties, low cost, good casting ability as well as corrosion resistance[9−11]. However, due to the unstable dislocations and Si phase, whose coefficient of thermal expansion (CTE) is much lower than that of aluminum, ZL114A demonstrates poor dimensional stability[12−15]. Heat treatment is an effective method to improve the microstructure and properties. Unfortunately, previous researches about heat treatment are mainly for strength and plasticity[16−18], while heat treatment for dimensional stability has not yet been developed.

In the present work, heat treatment for improving dimensional stability of Zl101A alloy is studied, and the effect of heat treatment on microstructure, micro-yield strength (MYS) and dynamic dimensional stability (DDS) are discussed.

## 2 Experimental

Table 1 shows the composition of ZL114A alloy plate used in the present experiment. Six heat treatment processes were designed for evaluation, as listed in Table 2. Salt solution treatment was employed in molten salt, in which the mixture of $KNO_2$ and $NaNO_2$ with a ratio of 1:1 were used as molten salt. Aging was carried out after quenching immediately. Temperature accuracy of salt-bath furnace and drying oven was within ±1 °C.

After mechanical polishing and etching with 10 mL HF+5 mL HCl+5 mL $HNO_3$+380 mL $H_2O$ solution, optical microstructure (OM) was observed by OLYMPUS

**Table 1** Composition of ZL114A alloy plate used (mass fraction, %)

| Si | Fe | Mg | Ti | Cu | Mn | Sn | Pb | Be |
|----|----|----|----|----|----|----|----|----|
| 6.92 | 0.26 | 0.58 | 0.12 | 0.014 | 0.078 | <0.001 | <0.001 | <0.001 |

**Table 2** Heat treatment process of ZL114A alloy

| No. | Heat treatment process |
|-----|------------------------|
| 1 | (540 °C, 12 h)+water quench(60−100 °C)+ (160 °C, 6 h) |
| 2 | (550 °C, 12 h)+water quench(60−100 °C) + (160 °C, 6 h) |
| 3 | (560 °C, 12 h)+water quench(60−100 °C) + (160 °C, 6 h) |
| 4 | (550 °C, 4 h)+water quench(60−100 °C) + (160 °C, 6 h) |
| 5 | (550 °C, 12 h)+water quench(60−100 °C) + (220 °C, 6 h) |
| 6 | (550 °C, 12 h)+water quench(60−100 °C)+ (280 °C, 6 h) |

PMG$_3$ optical microscope. Further observation was carried out on Philips CM-12 transmission electron microscope (TEM) with an accelerated voltage of 120 kV. Thin foils were prepared by mechanical polishing followed by twin jet electrolytic thinning, where 33%

HNO$_3$+67% CH$_3$OH mixing solution was used at −20 °C under 20 V. MYS and DDS of ZL114A aluminum alloy were investigated by tensile testing and thermal cycling on-line measuring method, respectively, where the samples were cycled between 20 °C and 150 °C for 10 complete cycles with a heating and cooling rate of 8 °C/min. The helium atmosphere was maintained at a flow rate of 50 mL/min and liquid nitrogen was used as coolant. Before each cycle, the samples were maintained at 20 °C and held for 25 min to ensure the equilibrium of temperature.

# 3 Results and discussion

## 3.1 Effect of solid solution process on microstructure and properties of ZL114A alloy

Fig.1 shows the optical microstructures of ZL114A alloy under different solution temperatures (as-cast, 540 °C, 550 °C and 560 °C). In as-cast alloy (Fig.1(a)), the smaller black bone-shape phases are Mg$_2$Si, while the larger ones are AlFeMnSi phases that are impurity phase.

The solution temperature of Mg$_2$Si is 478−525 °C, depending on Mg content of the alloy. It is obvious that Mg$_2$Si has been fully dissolved into α(Al) phase and no Mg$_2$Si phase is observed under solid solution temperature of 540, 550 and 560 °C (Figs.1(b), (c) and (d)). After solid solution treatment at 540 °C, the eutectic Si phase becomes coarse with massive and long rod
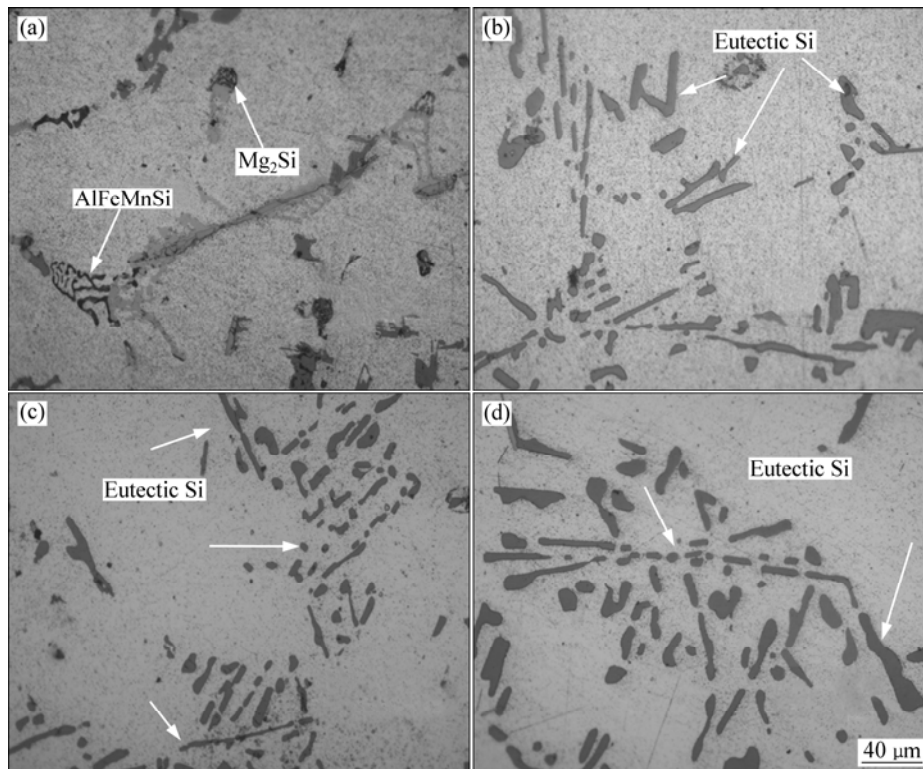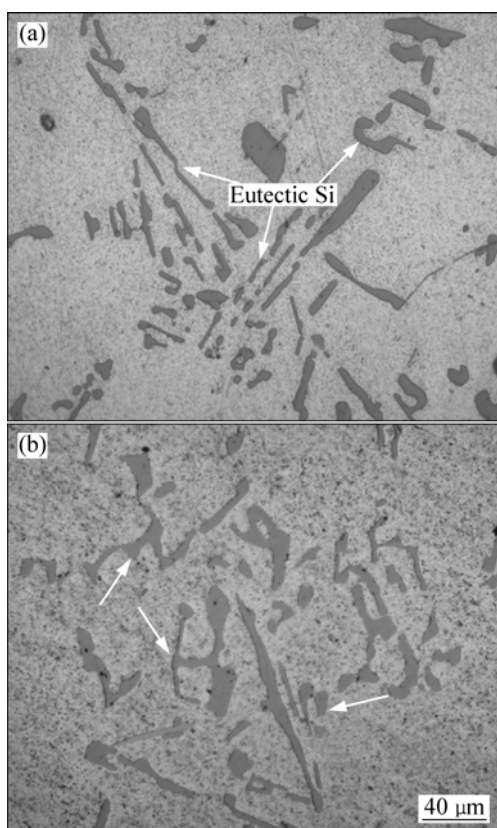


**Fig.1** Optical microstructures of ZL114A alloy under different solid solution temperatures: (a) As-cast; (b) 540 °C; (c) 550 °C; (d) 560 °C

shape. At 550 °C, Si phase is smaller with less massive and needle-like shape than that at 540 °C. At 560 °C, Si is spheroidized. After solid solution treatment, eutectic Si phase disconnects into blocky. Although a small amount of long rod Si phase is still observed, the spheroidization degree of Si increases with the increase of solid solution temperature.

Fig.2 shows the optical microstructures (OM) of ZL114A alloy under different solution time (4 h and 12 h at 550 °C). Eutectic Si is coarse with long rod, blocky and irregular shape and no fine globular Si phase is observed after the alloy is solution treated at 550 °C for 4 h. Although long rod Si phase still exists, the spheroidization degree of eutectic Si increases after solid solution treatment at 550 °C for 12 h. It is also indicated that, under low solid solution temperature, even with a high solution temperature, only a small amount of Si change to small blocky shape, while most of them keep rod shape.

The micro-yield strength (MYS) of ZL114A alloy after different solid solution treatment is listed in Table 3. It is obvious that the MYS of which the deformation is $10^{-5}$ reaches maximum at 550 °C (220.3 MPa), and at 540 °C and 560 °C is 197.4 MPa and 149.6MPa, respectively. The microstructure observation revealed that the massive and long rod shape eutectic Si is less at 550 °C than at 540 °C (shown as Figs.1(b) and (c)), and



**Fig.2** Optical microstructures of ZL114A alloy with different solid solution time at 550 °C: (a) 4 h; (b) 12 h

**Table 3** MYS of ZL114A alloy after different solid solution treatments (MPa)

| Different solution temperature | | | Different solution time | |
|---|---|---|---|---|
| 540 °C, 12 h | 560 °C, 2 h | 550 °C, 12 h | 550 °C, 4 h | 550 °C, 12 h |
| 197.4 | 149.6 | 220.3 | 144.4 | 220.3 |

the eutectic Si is smaller at 550 °C than at 560 °C (shown as Figs.1(c) and (d)). It is revealed that the less the massive and long rod shape Si phase or the smaller Si phase is, the higher the MYS obtained will be. Furthermore, MYS of ZL114A alloy after long solution time (220.3 MPa at 550 °C for 12 h) is higher than that at short time (144.4 MPa at 550 °C for 4 h). Microstructure observation reveals that the spheroidization degree of eutectic Si increases with prolonging of solution time (see Figs.2(a) and (b)). It is indicated that the higher the spheroidization degree is, the higher the MYS will be.

### 3.2 Effect of aging temperature on microstructure and properties of ZL114A alloy

As mentioned above, under the premise of without overburn and full solid solution of alloying element, high solution temperature and long solution time should be adopted. Thus, (550 °C, 12 h) was selected as solution process. After water quenching, aging treatment was carried out for 6 h at 160, 220 and 280 °C, respectively.

Fig.3 gives the TEM microstructures of ZL114A alloy after aging treatment. Generally, precipitation of Al-Si-Mg alloy occurs by following steps: supersaturated $\alpha \rightarrow$ GP zone $\rightarrow \beta'$ phases (Mg$_2$Si) $\rightarrow \beta$ phases (Mg$_2$Si). As shown in Fig.3, precipitation in ZL114A alloy transforms from GP zone (160 °C, Fig.3(a)), metastable $\beta'$ phase (220 °C, Fig.3(b)) to stable Mg$_2$Si phase (280 °C, Fig.3(c)) with increasing aging temperature.

MYS of ZL114A alloy after aging treatment is listed in Table 4. MYS decreases from 220.3 MPa after aging at 160 °C to 41.3 MPa at 280 °C. The formation of precipitate with best size and distribution in the alloy, which could improve MYS, is the objective of the aging treatment. However, the effects of precipitates are different. GP zone (160 °C, Fig.3(a)) is completely coherent with matrix, $\beta'$ phase (220 °C, Fig.3(b)) is semi-coherent with matrix and $\beta$ phase (280 °C, Fig.3(c)) is non-coherent with matrix. The precipitates in the alloy impede dislocation movement by forcing the dislocations to either cut through the precipitated particles or go around them, while the hardening way depends on precipitates' size and coherent relation with matrix. It is obvious that the coherent strengthening is the most effective way to improve MYS of ZL114A alloy. The smaller the GP zone or $\beta'$ phase is, the better the strengthening effect is. However, with the precipitation of $\beta$ phase (Mg$_2$Si), MYS decreases greatly.
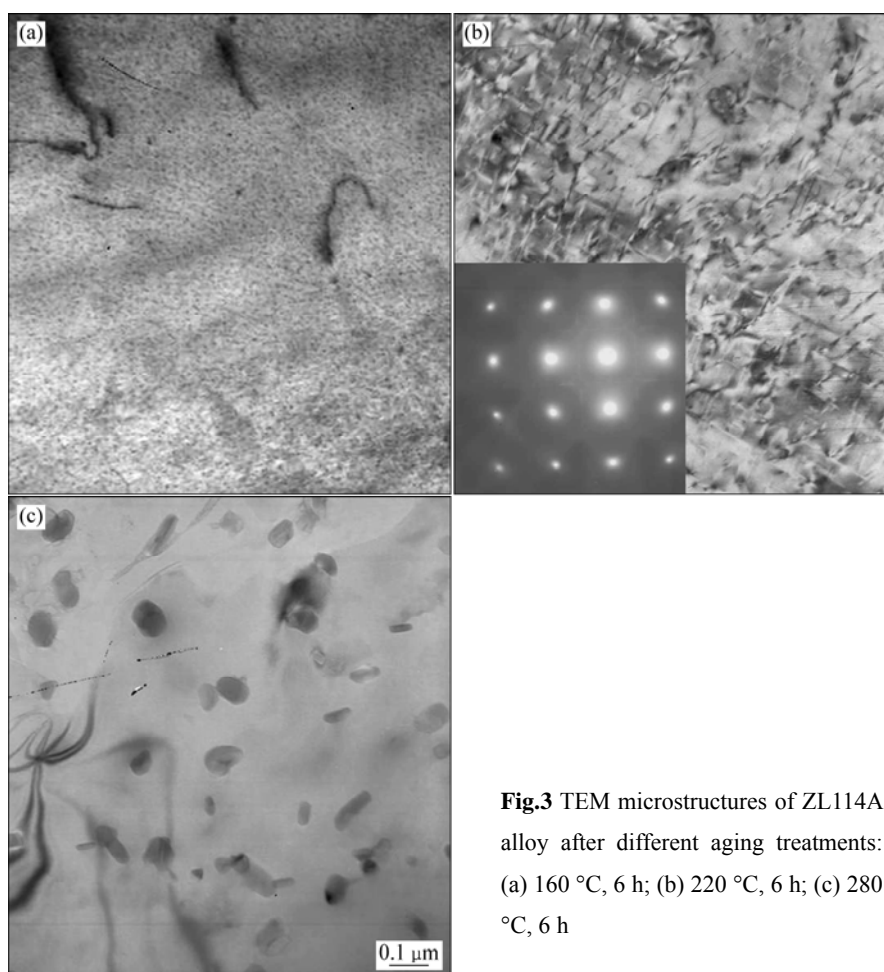
**Fig.3** TEM microstructures of ZL114A alloy after different aging treatments: (a) 160 °C, 6 h; (b) 220 °C, 6 h; (c) 280 °C, 6 h

**Table 4** MYS of ZL114A alloy after aging treatment for 6 h (MPa)

| At 160 °C | At 220 °C | At 280 °C |
|-----------|-----------|-----------|
| 220.3 | 172.6 | 41.3 |

### 3.3 Effect of aging temperature on DDS of ZL114A alloy

Fig.4 presents the DDS testing results of ZL114A alloy aging treated under different temperatures. Minute dimensional variation of sample resulting from precipitation and macro-residual stress was tested under the condition of temperature alternation and no loading. It is revealed from three DDS curves in Fig.4 that the dimension of sample after aging at 160 °C, whose precipitates are GP zones, becomes longer. DDS of sample after aging at 220 °C, whose precipitates are $\beta'$ phases, is bad and DDS curve does not reach stable after 10 cycles, while still descends. It is indicated that DDS of sample after aging at 280 °C, whose precipitates are stable $Mg_2Si$ phases, is the best.

GP zone is the main precipitate of ZL114A alloy when aging at 160 °C. During thermal cycling, some GP zones grow up to $\beta'$ phase with the increase of cycles.
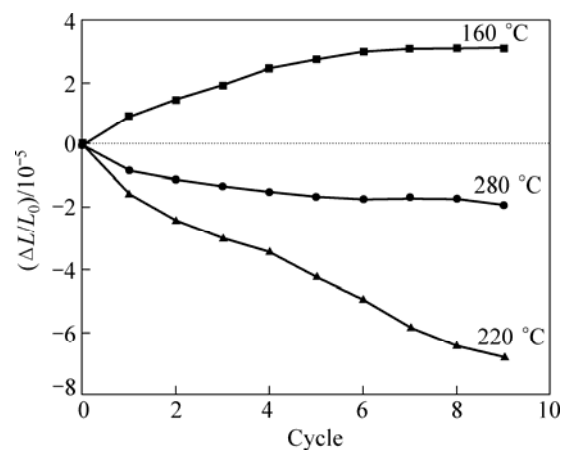


**Fig.4** DDS of ZL114A alloy under different aging temperature (without first cycle)

The different specific volume of matrix and precipitates result in the variation of length. Some GP zones grow up and coherence strain strengthens, which causes the increase of length. Although the formation of $\beta'$ phase could relax the residual stress during cycling, the growth of GP zone and strengthening of coherence strain result

in the variation of length. $\beta'$ phase is the main precipitate of ZL114A alloy when aging at 220 °C. The strengthening of coherence strain is weakened and the residual stress generated by increasing the thermal mismatch then becomes the main factor. Eventually, the $\beta'$ phase is replaced by stable spherical $\beta$ phase (Mg$_2$Si) when aging at 280 °C. Although MYS of the sample after aging at 280 °C is very low (41.3 MPa), indicating that dimension is very sensitive to stress, these stable spherical Mg$_2$Si would generate uniform stress field. The offset of stress leads to low macro-residual stress. Even though the MYS of sample after aging at 220 °C is 3 times that at 280 °C, DDS of the latter is better than that of the former. Therefore, micro-yield strength, which is used for characterization of the dimensional stability currently, is the plastic deformation resistance at initial stage under load. It cannot characterize the dimensional stability comprehensively under the condition of unstable phase and microstructure. DDS under alternative temperature should also be tested cooperatively for better evaluation of dimensional stability. The effects of precipitates on dimensional stability are listed in Table 5.

**Table 5** Dimensional stability evaluation of ZL114A alloy

| Precipitate | Phase stability | Stress stability | MYS | DDS |
|---|---|---|---|---|
| GP zone | Unstable | − | Highest | Good |
| $\beta'$ phase | Metastable | Unstable | High | Worst |
| Mg$_2$Si | Stable | − | Lowest | Best |

## 4 Conclusions

1) Solution temperature shows great effect on the morphology of eutectic Si. The spheroidization degree of Si increases while massive and long rod phase decreases with solid solution temperature. The longer the solution time is, the smaller the massive and longer rod Si phases are. The less the massive and long rod shape Si phase or the smaller Si phase is, the higher the MYS can be obtained.

2) Coherent strengthening is the most effective way to improve MYS of ZL114A alloy. The smaller the GP zone or $\beta'$ phase is, the better the strengthening effect is. However, with the precipitation of $\beta$ phase (Mg$_2$Si), MYS decreases greatly.

3) DDS of ZL114A alloy with stable $\beta$ phase (Mg$_2$Si) is better than that with GP zone and $\beta'$ phase. Micro-yield strength is the plastic deformation resistance at initial stage under load, but it cannot characterize the dimensional stability comprehensively under unstable phase and microstructure. DDS under alternative temperature should also be tested cooperatively for better evaluation of dimensional stability.

## References

[1]    WANG Q G, DAVIDSON C J. Solidification and precipitation behaviour of Al-Si-Mg casting alloys [J]. Journal of Materials Science, 2001, 36(3): 739−750.

[2]    BIROL Y. Semi-solid processing of the primary aluminium die casting alloy A365 [J]. Journal of Alloys and Compounds, 2009, 473(1/2): 133−138.

[3]    CESCHINI L, MORRI A, GAMBERINI A, MESSIERI S. Correlation between ultimate tensile strength and solidification microstructure for the sand cast A357 aluminium alloy [J]. Materials and Design, 2009, 30(10): 4525−4531.

[4]    ZHU Z J, WANG H W, ZENG S Y. The effect of heat treatment on the properties of A357 alloy [J]. Cast, 2005, 54: 978−980.

[5]    CHEN Z W, JIE W Q. Effect of Mg content on microstructure and mechanical properties of Al-Si-Mg casting alloy [J]. Journal of Materials Science and Engineer, 2004, 22(5): 647−652.

[6]    LI W C, ZOUY Z, ZENG J M, GAN W K. Effect of solid solution treatment on microstructure and mechanical properties of ZL114A alloy [J]. Cast, 2008, 57(6): 565−568.

[7]    ALEXOPOULOS N D, PANTELAKIS S G. Quality evaluation of A357 cast aluminum alloy specimens subjected to different artificial aging treatment [J]. Materials and Design, 2004, 25: 419−430.

[8]    WANG Q G. Microstructural effects on the tensile and fracture behavior of aluminum casting alloys A356/357 [J]. Metallurgical and Materials Transactions A, 2003, 34(12): 2887−2899.

[9]    ZHANG R J, WANG X Y, JIE W Q. Solute partition behavior and its influences on solidification process of Al-Si-Mg alloy [J]. Transactions of Nonferrous Metals Society of China, 2003, 13(6): 1484−1487.

[10]   LI X L, HAO Q T, JIE W Q, ZHOU Y C. Development of pressure control system in counter gravity casting for large thin-walled A357 aluminum alloy components [J]. Transactions of Nonferrous Metals Society of China, 2008, 18(4): 847−851.

[11]   ALEXOPOULOS N D, TIRUAKIOĞLU M. Relationship between fracture toughness and tensile properties of A357 cast aluminum alloy [J]. Metallurgical and Materials Transactions A, 2009, 40(3): 702−716.

[12]   REN S B, HE X B, QU X H, HUMAIL I S, LI Y. Effect of Mg and Si in the aluminum on the thermo-mechanical properties of pressureless infiltrated SiC$_p$/Al composites [J]. Composites Science and Technology, 2007, 67(10): 2103−2113.

[13]   ZHANG Q, WU G H, JIANG L T, CHEN G Q. Thermal expansion and dimensional stability of Al-Si matrix composite reinforced with high content SiC [J]. Materials Chemistry and Physics, 2003, 82(3): 780−785.

[14]   SMAGORINSKI M E, TSANTRIZOS P G. Development of light composite materials with low coefficients of thermal expansion [J]. Materials Science and Technology, 2000, 16(7/8): 853−861.

[15]   ALEXOPOULOS N D, PANTELAKIS S G. Quality evaluation of A357 cast aluminum alloy specimens subjected to different artificial aging treatment [J]. Materials and Design, 2004, 25(5): 419−430.

[16]   PEDERSEN L, ARNBERG L. The effect of solution heat treatment and quenching rates on mechanical properties and microstructures in AlSiMg foundry alloys [J]. Metallurgical and Materials Transactions A, 2001, 32(3): 525−532.

[17]   BERRYT S. Study of the effects of volume fraction, size and shape of solution particles on mechanical properties in Al-Si alloy using finite element method [J]. AFS Transaction, 1987, 37(12): 824−828.

[18]   SHIVKUMAR S, KELLER C, APELIAN D. Aging behavior in cast Al-Si-Mg alloys [J]. AFS Transactions, 1990, 98: 905−910.

**(Edited by LAI Hai-hui)**